J Electroceram (2010) 25:218–222
DOI 10.1007/s10832-010-9618-3

# Fabrication of three-dimensional electromagnetic band-gap structure with high-K dielectric ceramics by rapid-prototyping

**Wei Dai · Hong Wang · Minjie Wang · Zhiyuan Shen · Dichen Li · Di Zhou · Jianzhang Shi**

Received: 9 June 2010 / Accepted: 13 August 2010 / Published online: 1 September 2010


**Abstract** Three-Dimensional diamond structure electromagnetic band-gap (EBG) structures containing high-K dielectric ceramic $Bi(Nb_{0.992}\ V_{0.008})O_4$ (BVN) fabricated by rapid-prototyping (RP) technique were investigated. The simulations based on finite element method (FEM) were employed to model the band diagram. The influences of structure dimensions, aspect ratio and permittivity contrast on the band gap width were studied. The optimal band gap width EBGs were fabricated and investigated experimentally. EBG structures composed of epoxy resin diamond lattice and inverse-diamond lattice made of high-K BVN ceramic with silica gel were fabricated by RP method. The transmission characteristics of the EBG structures were measured by transmission/reflection (T/R) methods with a vector network analyzer. Obvious wide band-gaps of two EBGs with different lattice parameters were observed in the curve of transmission characteristics, which agreed well with the simulation results.

**Keywords** EBG · Diamond structure · BVN ceramic · RP technique · FEM · T/R method

## 1 Introduction

In recent years, considerable attentions have been focused on artificial electromagnetic materials such as photonic crystals [1], electromagnetic band-gap (EBG) structures [2, 3], and double negative (DNG) materials [4]. The EBGs, which were periodically arranged in space with dielectric materials, are also considered as a kind of photonic crystals working at microwave frequency range. The EBGs have been developed from two-dimensional (2D) structures to simple three-dimensional (3D) structures and to more complicated 3D structures and only in 3D EBG structures a complete band-gap can appear since the first Brillouin zone of 3D EBGs is nearly spherical in shape. Various 3D EBG structures such as Yablonivite [5], woodpile [6–8], opal [9], and diamond structures [10] have been fabricated. In all these EBGs, the diamond structure is known as an ideal structure with a complete band-gap and the diamond structure was chosen in this work.

Generally speaking, the band-gap width depends on high / low permittivity contrast of the two constituent dielectric materials. The larger the high /low permittivity contrast is, the wider the band-gap width will be. However, if the permittivity of the high-K part is too large, the band center frequency will shift to low frequency and this will decrease the band-gap width. What more, the band-gap width is also related to the aspect ratio, which is the ratio of the radius (r) of the diamond lattice rod and period lattice constant (a). How to get an optimal result is a question. By fixing the aspect ratio at an optimal point and changing the permittivity of the high-K part, the broadest band-gap width can be got. In this work, a new method using microwave dielectric ceramics with moderate permittivity and a felicitous aspect ratio (r/a) to fabricate EBGs was proposed to enlarge the band-gap width.

To study the propagation properties of electromagnetic wave in EBGs, many numerical computation methods have been developed and used. The widely used conventional ones include plane-wave method [11], transfer matrix method [12], and finite-difference time-domain (FDTD)

W. Dai · H. Wang (✉) · Z. Shen · D. Zhou · J. Shi
Electronic Materials Research Laboratory, Key Lab of the Ministry of Education, Xi'an Jiaotong University, Xi'an 710049, People's Republic of China
e-mail: hwang@mail.xjtu.edu.cn

M. Wang · D. Li
Rapid-prototyping Engineering Centre of the Ministry of Education, Xi'an Jiaotong University, Xi'an 710049, People's Republic of China

method [13]. Recently, a new method based on finite element method (FEM) is used to calculate the propagation properties of EBGs. The FEM based software Ansoft HFSS was used to calculate the band diagram of 3D EBGs in this work.

To fabricate EBGs, a lot of technologies have been used. The popular ones are microelectronics processes, such as silicon lithography, wafer fusion and etching, but these are more appropriate for terahertz and photonic wavelength applications. For EBGs, working at microwave and millimeter wave frequency ranges, these sophisticated microfabrication techniques are too costly. Alternative methods are building up the crystal rather than to remove materials to form the required structures, such methods including embossing, self-pulling, and self-organized EBGs. Rapid-prototyping (RP) technique is a typical method of additive fabrication which is suitable for EBG fabrication. The structure model is firstly designed by CAD software, and then the RP machine will fabricate samples according to the designed model. The 3-D diamond structure photonic crystals and its various modifications such as the inverse and graded lattice structures fabricated from a photopolymer epoxy resin containing $TiO_2$-based ceramic particles by using stereolithography have been investigated by Kirihara et al. [10, 14, 15]. However, no explicit relationship between the structure dimensions or aspect ratio and band gap width has been shown for the diamond structure probably because of the limit of the simulation method.

In this study, 3D diamond structure electromagnetic band-gap (EBG) structures containing high-K dielectric ceramic $Bi(Nb_{0.992}\ V_{0.008})O_4$ [16] (BVN) fabricated by rapid-prototyping (RP) technique with gel-casting were designed and investigated. A series of simulation were carried out to study the influences of structure dimensions and aspect ratio and permittivity contrast on the band gap width. The transmission characteristics of the EBG structures were measured and discussed.

## 2 FEM simulations

All of the macroscopic electromagnetism, including the propagation of electromagnetic wave in an EBG structure, is governed by the four macroscopic Maxwell equations [1]. The four Maxwell equations can be expressed as a single differential equation:

$$\nabla \times \left(\frac{1}{\varepsilon(r)}\nabla \times H(r)\right) = \left(\frac{\omega}{c}\right)^2 H(r) \tag{1}$$

$\varepsilon(r) = \varepsilon(r + la)$ is the permittivity distribution in EBGs, where $l$ is an integer and $a$ is the lattice constant. This is the characteristic equation from which the band diagram is created. It has been known that the Bloch theorem in solid-state physics can be generalized from this equation. Therefore, the solution of Eq. 1 has the form of Bloch wave:

$$H_k(r) = e^{i(k\cdot r)}u_k(r) \tag{2}$$

Where the function $\boldsymbol{u_k(r)}$ shares the same translational symmetries as $\varepsilon(\boldsymbol{r})$. Substituting the Block wave (2) back into Eq. 1, an eigenvalue equation is got from which the band diagram can be deduced. The band diagram has the form of $\omega_n(\boldsymbol{k})$, which is parallel to the energy band diagram $\varepsilon_n(\boldsymbol{k})$ in solid state electronics. The wave vector $\boldsymbol{k}$ is chosen to label different Block waves. For each value of $\boldsymbol{k}$, an infinite set of modes with discrete frequencies $\omega$ exist, which are then identified by the band index $n$ [17].

Figure 1(a) shows the unit cell model built to calculate the band diagram of the diamond EBG. It has the shape of dodecahedron and contains four interconnected columns. The interconnection point is corresponding to the position of grid point in the diamond lattice. A real diamond lattice can be obtained by expanding this unit cell in space. Figure 1(b) shows the first Brillouin zone of the diamond lattice. It can be seen that both unit cell and the first Brillouin zone belong to point group $O_h$.

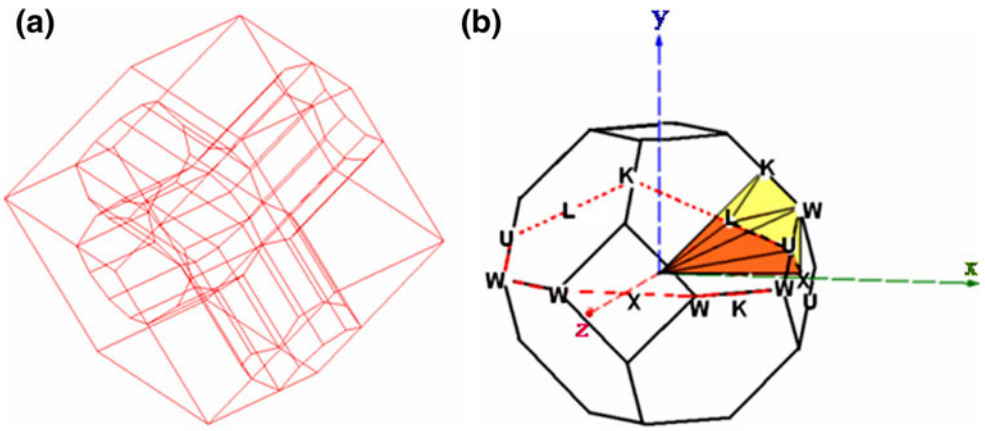


**Fig. 1** (**a**) The Wigner-Seitz unit cell of the diamond structure lattice (**b**) Irreducible Brillouin zone of the diamond structure lattice

FEM based software Ansoft HFSS was adopted to calculate the band diagram. The six pairs of parallel opposite planes of the dodecahedron were assigned with master/slave boundary conditions. A unit cell set with master/slave condition is equivalent to the 3D lattice spanning all around the space. Figure 2 gives simulated relationship between the aspect ratio r/a and the relative band width $\Delta\omega/\omega_{mid}$ which is the ratio of band-gap width and the center frequency of the band. From Fig. 2, it can be found that the relative band-gap width increases simultaneously with the aspect ratio less than 0.37 and then falls with the aspect ratio increasing. This result shows that the relative band-gap width reaches largest at the point of aspect ratio 0.37. By fixing the aspect ratio at 0.37 and changing the permittivity of the high-K part, the broadest band-gap width can be got by simulations. Based on this result, an EBG structure with lattice constant 10 mm and the radius of column 3.7 mm was designed and simulated. All the six calculated eigenfrequencies were normalized and the eigenfrequencies corresponding to different wave vector $\boldsymbol{k}$ were plotted to form a complete band structure. $\boldsymbol{k}$ is chosen to vary along several special directions in Brillouin zone, namely Γ- L- U- X and Γ- X- W- K as shown in Fig. 1(b). In the simulations, the low-K part used photosensitive resin (dielectric constant $\varepsilon_r$=4.49) and it was found the band width would be the largest when the permittivity of the high-K part was around 25. A complete wide band-gap can be got from 11.62 GHz to 14.52 GHz (0.387 to 0.484 in the normalized frequency) as shown in Fig. 3(a). In order to further validate the correctness of the result and investigate the changing of band-gaps with the dimension, another EBG whose dimension was 1.25 times of the former one was also simulated and a complete band-gap can be got from 10.14 GHz to 12.19 GHz (0.423 to 0.508 in the normalized frequency) as shown in Fig. 3(b).

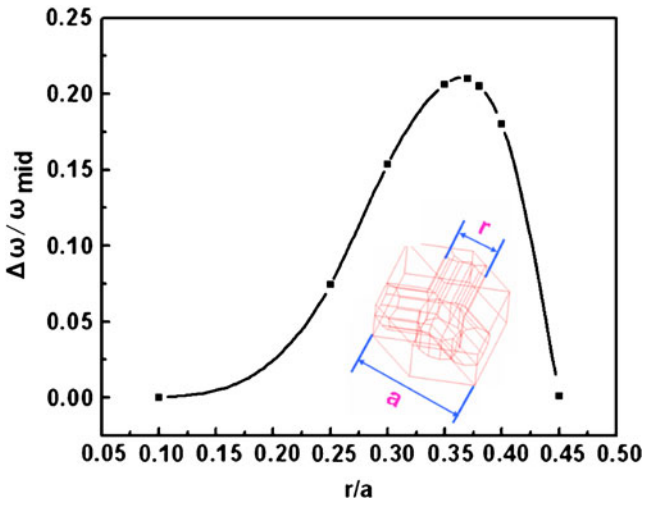


**Fig. 2** The relationship between the relative band-gap width and the aspect ratio

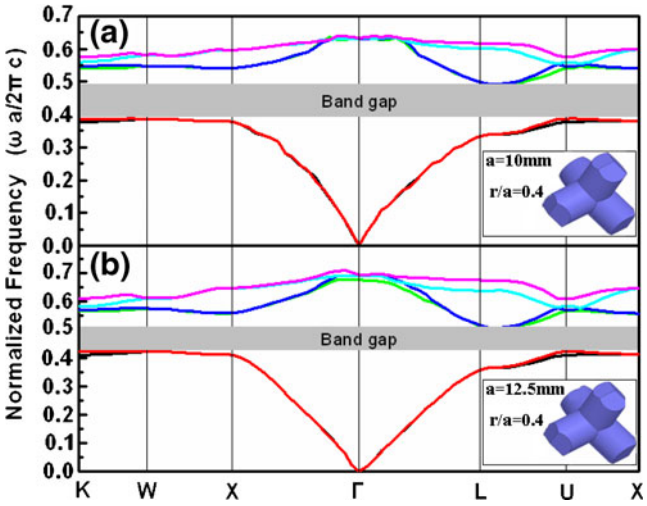


**Fig. 3** (**a**) The simulation results of the band diagram of the electromagnetic wave in EBG with the lattice constant of 10 mm. The results exhibit first six frequency modes in six different wave vector directions. In the inset, the unit cell with r/a of 0.37 and lattice constant of 10 mm is shown. (**b**) The simulation results of the band diagram of the electromagnetic wave in the EBG with the lattice constant of 12.5 mm. The unit cell is shown in the inset with r/a of 0.37 and lattice constant of 12.5 mm

## 3 Experimental

According to the simulation results, the 3D EBGs were fabricated by RP technique. First, the EBGs CAD models with the diamond structure expanding from the unit cell were generated by Ansoft HFSS. The CAD models of boxes to accommodate the EBGs inside with the size rightly matching the EBGs were also made by Ansoft HFSS. The EBG and the box molds were then fabricated by RP machine according to the designed CAD models. The size of the molds for the two different EBG structures were designed as 30 mm×20 mm×45 mm and 40 mm×30 mm×60 mm to ensure them large enough to be cut for the measurement.

The liquid resin of a photosensitive epoxy was used to fabricate the diamond structure molds and boxes by a RP machine (Hengtong, SPS450B, Xi'an, China). A laser beam was scanned across the surface of the epoxy resin based on the CAD data. The epoxy was solidified layer by layer through photopolymerization with single layer as thin as 100 μm, eventually forming a 3D structure. The diameter of the laser spot is 100 μm and the scanning speed is 90 mm/s. The dimensional accuracy of the structure was within 0.1%.

After the diamond structure molds and the boxes were fabricated, the silica gel slurry fully mixed with BVN ceramic powder at the ratio of 43:57 was cast into the box to about a half volume. Then putting the EBG molds into the boxes and pressing the systems slightly, the slurry

gradually permeated into the interstices of the diamond structure molds. The samples were kept still for 2 h and then evacuated under −0.09 MPa for degassing. The desiccation process was under −50°C in order to make the water changing into ice which sublimates at a higher temperature. By this way, the cracks and the air pores in the EBGs can be reduced to the lowest that would effectively improve the dielectric constant of the high-K part in the EBGs. The dielectric permittivity of the high-K part in the EBGs is measured as 25.45.

Removing the crust boxes, the EBG structures were obtained, which were composed of epoxy resin diamond lattice and the inverse-diamond high-K BVN ceramic powder with silica gel part. The edge margin parts not fully filled were cut off. The final EBG prototypes with the lattice constant of 10 mm and 12.5 mm are shown in the insets of Fig. 4(a) and (b).

## 4 Results and discussions

Figure 2 shows the relationship between the relative band-gap width and the aspect ratio. It can be found that the relative band-gap width increases with the increasing of the aspect ratio at first. When the aspect ratio reaches 0.37, the relative band-gap width is biggest. If the aspect ratio goes on increasing, the relative band-gap width will decrease. The aspect ratio 0.37 is the optimal point.

Figure 3 shows the simulation results of the two EBGs with the lattice constant of 10 mm (Fig. 3(a)) and 12 mm (Fig. 3(b)). A complete band-gap can be found from 0.387 to 0.484 in the normalized frequency (11.62 GHz to 14.52 GHz) as shown in Fig. 3(a) for the EBG structure

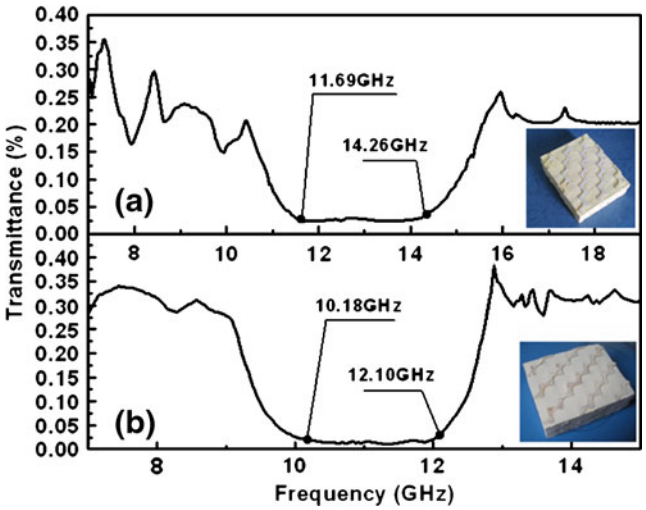


**Fig. 4** (**a**) The measured result of the first EBG sample. The first sample with the lattice constant of 10 mm is shown in the inset. (**b**) The measured result of the second EBG sample. The second sample with the lattice constant of 12.5 mm is shown in the inset

with the lattice constant of 10 mm. For the EBG with lattice constant of 12 mm, the band-gap is from 0.423 to 0.508 in the normalized frequency (10.14 GHz to 12.19 GHz) as shown in Fig. 3(b).

Transmission/reflection (T/R) methods are widely used in the measurement of microwave properties of materials [18]. In the T/R method, the sample under test is inserted into a segment of transmission line, and the permittivity and permeability of the sample are derived from the scattering equations. T/R methods were used in this work to obtain the transmission parameters $|S_{21}|$ of the EBG samples in order to study its propagation properties. A rectangular waveguide working under $TE_{10}$ mode was chosen as the transmission line to reduce the transmission loss and measure the samples in a rectangular shape. The EBG samples were cut as the size of the waveguide aperture and inserted into the waveguide. Along the length direction of the waveguide, four periods of lattice was kept. The waveguide was connected with a network analyzer (HP 8720ES, Hewlett-Packard, Santa Rosa, CA) through two adaptors. Two rectangular waveguides (WR90 22.86 mm×10.16 mm and WR62 15.8 mm×7.9 mm, Hengda, Xi'an, China) working at different frequency range were used in the measurement. WR90 covers the frequency range 8.2–12.5 GHz. After the measurement in WR90, the samples were further cut to fit the aperture of the WR62 waveguide. WR62 covers the frequency range 11.9–18.0 GHz. The short circuit calibration using a regulator made of Cu slice was employed.

For T/R methods using the rectangular waveguide, the air gap, caused by imperfect match of the sample and the waveguide, is a serious uncertainty exciter [19]. The effect of air gap along the height is not as serious as that along the width since the excited $TE_{10}$ mode has a zero field at the short walls [17]. The air gap can form defects, which may generate localized modes in EBG and destroy the homogeneous, leading to inaccurate test results. Wilson et al. [19] pointed out that filling the air gap with conducting paste can nearly alleviate the effect caused by the air gap. The air gaps in this work were filled with room temperature silver paste and the smooth $|S_{21}|$ spectrums were obtained as shown in Fig. 4(a) and (b).

Figure 4 shows the transmission curves with an obvious band stop property at the frequency range from 11.69 GHz to 14.26 GHz for the first EBG structure with lattice constant of 10 mm (Fig. 4(a)) and from 10.18 GHz to 12.10 GHz for the second one with lattice constant of 12 mm (Fig. 4(b)). It is also noteworthy that the band edge is clear and sharp. The band-gap widths of both EBGs decrease a little in comparison of the simulation results as shown in Fig. 3 with the band-gap from 11.62 GHz to 14.52 GHz (0.387 to 0.484 in the normalized frequency) for the first EBG and 10.14 GHz to 12.19 GHz (0.423 to 0.508 in the normalized frequency) for the second EBG, which

are probably caused by the material itself. The transmission scattering parameter $|S_{21}|$ dropped more than −38 dB within the band-gap and this expresses the band gap properties are very good. At frequencies below and above the stop band, the transmission exhibits ripple structures, with an average value around –12 dB, which means the electromagnetic waves can propagate freely.

The band gap width to the mid-gap frequency ratios $\Delta\omega/\omega_{mid}$ are 12.6% and 17.2% for the two EBGs, respectively. The band-gap widths are much wider than the reported results in the relatived literature [14, 20–22]. In all of the reported results, the widest band-gap is 1.7 GHz. The much wider band-gap in this work attributes to the control of aspect ratio and permittivity contrast based on the simulation results.

Figure 4(a) and (b) show the band gap properties altering with the dimensions changing of the two samples. Fig. 4(a) shows the result of the sample with lattice constant of 10 mm, while the Fig. 4(b) shows the result of the second sample with lattice constant of 12.5 mm. From the two results, it can be found that with the increasing of the lattice constant of the sample, the band gaps will shift toward low frequency. This result verifies the theory presented by Joannopoulos et al. [1]. Engineering of EBG structures and lattice modifications is of importance for microwave and millimeter wave applications. For example, the microfabrication of complex micro-scale EBGs is quite difficult. But models can be easily made and tested in the microwave range, at the much larger length scale of centimeters.

The band gap and its width changing with the aspect ratio and permittivity contrast properties represent an important step towards the practical applications of EBG structures to microwave circuits and integrated devices.

## 5 Conclusions

In summary, a method to realize broad band-gap width EBG structures by adjusting the aspect ratio and the permittivity contrast of the high-K/low-K materials has been proposed. By fixing the aspect ratio at an optimal point and changing the permittivity of the high-K part, the broadest band-gap width can be found by simulation. Based on the simulation results, the practical EBG structures were fabricated and experimentally investigated. A fabricating method by rapid-prototyping technique was used to make sure the accurate fabrication of EBGs and the flexible adjusting of the constituent materials. This work represent an important step on fabricating complicated 3D EBGs with complete wide band-gaps by RP method with any materials. The broad band-gap widths were experimentally confirmed by transmission/reflection method measurements. Wide band-gap characteristics have been observed with the band gap from 11.69 GHz to 14.26 GHz for the first EBG structure (a=10 mm, r/a=0.37) and from 10.18 GHz to 12.10 GHz for the second one (a=12.5 mm, r/a=0.37). The results agreed well with the theoretical simulations by HFSS calculations. The RP method in making EBGs flexibly shows an effective way for EBGs perspective applications.

**Acknowledgement** This work was supported by NSFC project of China (60871044, 50835007), National 973 project of China (2009CB623302) and National Project of International Science and Technology Collaboration (2009DFA51820).

## References

1. J.D. Joannopoulos, R.D. Meade, J.N. Winn, *Photonic Crystals* (Princeton University Press, Princeton, 1995)
2. Y. Rahmat-Samii, H. Mosallaei, Eleventh Int. Conf. Antennas Propagat. **480**, 560–564 (2001)
3. D. Sievenpiper, L.J. Zhang, R.F.J. Broas, N.G. Alexoplous, E. Yablonovitch, IEEE Trans. Microwave Theory Tech. **47**(11), 2059–2074 (1999)
4. J.B. Pendry, Phys. Rev. Lett. **85**, 3966–3969 (2000)
5. E. Yablonovitch, T.J. Gmitter, K.M. Leung, Phys. Rev. Lett. **67** (17), 2295–2298 (1991)
6. E. Ozbay, A. Abeyta, G. Tuttle, M. Tringides, R. Biswas, C.T. Chan, C.M. Soukoulis, K.M. Ho, Phys. Rev. B. **50**, 1945–1948 (1994)
7. S. Noda, Physica. B. **279**, 142–149 (2000)
8. S.Y. Lin, J.G. Fleming, D.L. Hetherington, B.K. Smith, R. Biswas, K.M. Ho, M.M. Sigalas, W. Zubrzyckl, S.R. Kurtz, J. Bur, Nature **394**, 251–253 (1998)
9. Y.A. Vlasov, X.Z. Bo, J.C. Sturm, D.J. Norris, Nature **414**, 289–293 (2001)
10. S. Kirihara, Y. Miyamoto, K. Takenaga, M.W. Takeda, K. Kajiyama, Solid State Commun. **121**, 435–439 (2002)
11. H.S. Soezueer, J.W. Haus, R. Inguva, Phys. Rev. B. **45**(24), 13962–13972 (1992)
12. J.B. Pendry, A. MacKinnon, Phys. Rev. Lett. **69**(19), 2772–2775 (1992)
13. C.T. Chan, Q.L. Yu, K.M. Ho, Phys. Rev. B. **51**(23), 16635–16642 (1995)
14. S. Kirihara, M.W. Taketa, K. Sakoda, Y. Miyamoto, Solid State Commun. **124**, 135–139 (2002)
15. H.Q. Yin, S. Kirihara, Y. Miyamoto, J. Am. Ceram. Soc. **87**(4), 598–601 (2004)
16. D. Zhou, H. Wang, X. Yao, Y. Liu, J. Electroceram. **21**, 469–473 (2008)
17. Z.Y. Shen, H. Wang, J.Z. Shi, X. Yao, J. Am. Ceram. Soc. **91**(9), 2892–2896 (2008)
18. L.F. Chen, C.K. Ong, C.P. Neo, V.V. Varadan, V.K. Varadan, *Microwave Electronics Measurement and materials Characterisation* (Wiley, West Sussex, 2004)
19. S.B. Wilson, IEEE Trans. Microwave Theory Tech. **36**(4), 752–756 (1988)
20. Z.T. Liu, S. Kirihara, Y. Miyamoto, D. Zhang, J. Am. Ceram. Soc. **89**(8), 2492–2495 (2006)
21. T. Nakagawa, K. Kageyama, N. Wada, Y. Sakabe, S. Kirihara, Y. Miyamoto, J. Am. Ceram. Soc. **90**(4), 1112–1115 (2007)
22. S. Kanehira, S. Kirihara, Y. Miyamoto, J. Am. Ceram. Soc. **88**(6), 1461–1464 (2005)